

Phenomena, mechanisms and structures in wished and unwished foams in matter of biological origin

Bernhard Gattermig^a, Anuhar Osorio Nesme^a, Lidia Almazán Torres^a,
Julian Thünnesen^a, Tobias Beck^a, Christopher McHardy^b, Thomas
Bernstein^b, Giovanni Luzi^c, Thomas Stahl^c, Cornelia Rauh^{b,c}, *Antonio
Delgado^{a,c}

^a*Institute of Fluid Mechanics, FA Universität Erlangen, Cauerstr. 4, 91058 Erlangen, Germany*

^b*Food Biotechnology and Process Engineering, TU Berlin, Königin-Luise-Str. 22, 14195 Berlin, Germany*

^c*German Engineering Research and Development Center LSTME Busan, 1276 Jisa-Dong, Gangseo-Gu,*

Busan 18-230, Republic of Korea

^a bernhard.gattermig@fau.de

ABSTRACT

Foams are available in numerous natural and technical processes. Consequently, there is a comprehensive scientific literature, which reports on some quite exotic phenomena, mechanisms and structures. As an introduction, this contribution intends to give a corresponding brief overview. Foams are non-equilibrium systems per se, in which the characteristic length scales change with advancing time within characteristic length scales (Wolf et al., 2016). However, this means that the existence of specific phenomena, mechanisms and structures depends on the number of Deborah. This increases the complexity of experiments (Zoheidi et al., 2017) and, accordingly, of modelling, simulation, prognosis and diagnosis of natural foams (Anderl et al., 2014c) as well as of the optimization of technical foams as this contribution will illustrate. With a focus on transport processes, for sake of convenience this contribution focuses on such foams, which play a major role in the individual's needs coverage. It includes foams in the fields of food and nutrition, pharmacy, medicine and human biology, personal care and wastewater treatment. Some foams turn out to be desirable. For example, many of the Haute cousin's specialties rely on the preference of most of the people of the light mouthfeel produced by foams while intraoral food intake. Therefore, specific food foam structures are designed and stabilized or more general for the specific goal functionalized. In other cases, foams represent a source of disturbances, such as when the function of a food production plants fails due to an excessive foam layer. Thus, this article discusses physical measures for the prevention, inhibition and control of disturbing foams from the point of view of the phenomena, mechanisms and structures to be influenced. On the other hand, this article uses the example of protein food foams to address how global quantities such as foamability and the behavior of foams under static and dynamic conditions can be predicted. An information technology hybrid that manages information from different sources provides such possibilities. The obtained results show that this is about 10% achieved with very

small errors in the maximum order of magnitude.

1. INTRODUCTION

Foams are dispersions of gas in liquid or solid that are stabilized by surfactants. They belong to a wide class of metastable nonequilibrium systems such as emulsions that rearrange and coarsen with time mainly by two mechanisms. First by Ostwald ripening, that is the diffusion of the dispersed phase from smaller bubbles into bigger ones driven by the Laplace pressure. The second mechanism is coalescence, which is caused by the rupture of the thin liquid film separating two adjacent bubbles. The characteristic time for this coarsening of foams spans a wide range from few seconds to many days. Foams applied in a variety of applications such as food and nutrition, pharmacy, medicine and human biology, cosmetics and wastewater treatment. In other cases, foams represent a source of disturbance, such as when the function of a production plants fails due to an excessive foam layer. In both cases of desired and unwanted foams, a profound knowledge of foam structure, stability and mechanical properties are a key factor for process design. The following chapter is intended to provide this basis. The article then proceeds with an introduction on modelling and numerical simulations of foam and closes with a practical description of selected applications.

2. STRUCTURE, MECHANISMS AND PHENOMENA

This description of foam properties follows the characteristic length scales from the micro/nanoscale for surface layers through the mesoscale, describing films and cells/bubbles to the macroscopic foam behavior.

Microscale. The formation of a free surface in liquid requires an input of energy, which is described by the surface tension γ multiplied by the surface area S . This tension is also responsible for the shape of a surface, a correlation described by the Young-Laplace law by after Pierre-Simon de Laplace (1749–1827) and Thomas Young (1773–1829):

$$\Delta P = \gamma \left(\frac{1}{R_1} + \frac{1}{R_2} \right) \quad \text{Eq. (1)}$$

Here, ΔP equals the pressure difference between both sides of the surface and R_i the principal radii. It can be seen that the pressure on the convex side of the surface will increase with smaller radii. This happens because the surface tension will try to reduce the curvature, aiming for an energetically beneficial flat surface. The effect causes individual gas compartments within a liquid to take on spherical shape in the absence of other forces. A foam is built up of many of these spheres, separated by films of varying thickness. Whenever two of these gas/liquid interfaces (e.g. two bubbles) approach beyond a critical separation distance or film thickness, van der Waals forces will cause them to merge¹ and thereby disrupt the film (De Gennes et al.,

¹ A bubble of volume $2V$ has a smaller surface area and thus less surface energy $E = \gamma \cdot S$ than two bubbles of volume V

2013). The formation of a stable foam thus requires the presence of a repulsive interface force, generated typically by surface active components (surfactants). These amphiphilic molecules adsorb at the interface in monolayers and align their hydrophobic section (tail of tensides) with the gas side and the hydrophilic part with the liquid. When the interfaces approach, the latter will be repelled by electrostatic forces, counterbalancing the attractive van der Waals forces². The resulting repulsion at equilibrium thickness is called disjoining pressure Π_d .

Possible candidates for such surfactants are the aforementioned amphiphilic molecules, e.g. sodium dodecyl sulphate (SDS), along with proteins, polymers or small particles. The adsorption behavior (or, more practically, surface tension as a function of surfactant concentration) can be described with the Gibbs fundamental adsorption equation (Eq. (2) (Gibbs, 1928) in conjunction with a suitable adsorption model. Arranged by increasing complexity, i.e. increasing surface loading, the most common models have been developed by Henry (Eq. (3), Henry 1803), Langmuir (Eq. (4), Langmuir 1917) and Frumkin (Eq. (5), Frumkin 1925).

$$\Gamma = -\frac{1}{RT} \frac{d\gamma}{d(\ln c)} \quad \text{Eq. (2)}$$

$$\gamma = \gamma_0 - RTKc \quad \text{Eq. (3)}$$

$$\Gamma = \Gamma_\infty \frac{c/a}{1 + c/a} \quad \text{Eq. (4)}$$

$$\Pi = -RT\Gamma_\infty \ln \left[1 - \frac{\Gamma}{\Gamma_\infty} \right] - a_F \left[\frac{\Gamma}{\Gamma_\infty} \right]^2 \quad \text{Eq. (5)}$$

Γ = Number of adsorbed molecules

R = Gas constant

T = Temperature

c = Bulk concentration

γ_0 = Surface tension of pure water

K = Henry constant

Γ_∞ = Maximum number of adsorbed molecules

a = Langmuir equilibrium adsorption constant

$\Pi = \gamma_0 - \gamma$ = Surface pressure

a_F = Alkyl chain interaction coefficient

Further models have been published recently, incorporating effects like reorientation (Fainerman et al., 1996), aggregation (Fainerman and Miller, 1996) or competition in surfactant mixtures (Fainerman et al., 2001; Fainerman and Miller, 2009). Of particular interest for food foams are adsorption models for proteins or protein/surfactant mixtures, as summarized in (Fainerman et al., 2003). Notable effects for such systems are a dependency of adsorption (ergo surface tension) on the pH-value and a competition between lower-molecular surfactants and proteins for interface coverage (Dan et al., 2012; Engelhardt et al., 2013, 2012; Wüstneck et al., 2012).

Since surfactant adsorption is a diffusion limited process, the mechanical properties of foam films are time dependent and change during film deformation. It is easily imaginable that the stretching of a film (i.e. increase in surface area) requires an additional transport of surfactants from the bulk to the interface. As this transport is limited by diffusion or adsorption / desorption barriers, the behavior of the film can be

² The *Van der Waals molecular interactions* or *dispersion molecular forces* as well as the *electrostatic* or *double layer forces* are called DLVO forces (both are long range forces), according to the DLVO theory (Derjaguin et al., 1987a; Verwey et al., 1948). These are accompanied by non-DLVO forces (Derjaguin et al., 1987b; Israelachvili, 2015) comprised of: steric surface forces, due to surfactant or polymer molecules; structural (solvation, hydration) surface forces which originate from modifications in the liquid structure adjacent to the film interfaces; as well as other surface forces, introduced by some authors. Most important for symmetric foam films are the steric repulsion interactions - long range for macromolecules, short range for small molecules.

described as two-dimensional viscoelastic (overview: (de Almeida and Mombach, 1997). In the limiting case of very low surfactant mobility or insolubility in the bulk (i.e. the number of molecules at the interphase is fixed), the elasticity is described by the Gibbs-Marangoni elastic modulus E_{GM} :

$$E_{GM} = - \left. \frac{d\gamma}{d(\ln\Gamma)} \right|_{eq} \quad \text{Eq. (6)}$$

In the general case, when the transport of surfactants from bulk to surface occurs in a similar timescale as the deformation, the complex dilatational elastic modulus $E_s^*(\omega)$ applies:

$$E_s^*(\omega) = E_s'(\omega) + iE_s''(\omega) \quad \text{Eq. (7)}$$

with: $E_s'' = \omega\eta_d$
 ω = Deformation frequency
 η_d = Surface dilatational viscosity

A high frequency ω leads to the limiting case for Gibbs-Marangoni modulus with $E_s' = E_{GM}$ and $E_s'' \approx 0$. In the opposite case, at low ω , surfactant transport is rapid enough to eliminate variations in concentration and thus surface tension, resulting in $E_s' = E_s'' = 0$.

In the Newtonian case, the same concept can be adapted in the case of shear forces, resulting in the 2D complex shear modulus:

$$G_s^*(\omega) = G_s'(\omega) + iG_s''(\omega) \quad \text{Eq. (8)}$$

with: $G_s'' = \omega\eta_s$
 ω = Deformation frequency
 η_s = Surface shear viscosity

The shear modulus is influenced mainly by the intermolecular interactions of surfactants at the interface, as opposed to the transport dominated elastic modulus. Surface elasticity has a direct influence on the foamability of a fluid. Surfactants will need to adsorb to the newly generated bubble surfaces quicker (characteristic time t_{ad}) than bubble growth and movement would lead to contact and merging of the films (t_{cont}). Thus, by tuning the system to achieve lower t_{ad} , bulk concentration and surfactant demand can be reduced in practical operation.

Another phenomenon driven by surfactant concentration gradients is the Marangoni effect. This is another example of a process in the microscale that influences macroscopic foam behavior (by limiting drainage - see section below). It occurs, when a bulk flow (e.g. due to gravity or temperature/density gradients) is superimposed on the surfactant diffusion. The bulk flow will drag adsorbed surfactants along, thus causing a concentration gradient inverse to the flow direction. Consequently, a surface diffusion flux and bulk mass flux ensue, in order to reduce the surfactant deficiencies. Both act against the original bulk flow, resulting in a reduction or – in extreme cases - complete elimination of the flux. The effect is actively employed in foam stabilization, as discussed later in chapter 4.

Mesoscale. The phenomena at the length-scale of individual bubbles (or cells) are responsible for the structure of the foam and determine the non-equilibrium behavior of foam. The characteristic parameter at this scale is the liquid volume fraction $\phi_l = V_l/V_{foam}$, discriminating the two regimes of dry foam ($\phi_l < 0,05$) and wet foam ($0,05 < \phi_l < \sim 0,3$). At liquid fractions larger than 0,3 the interaction between bubbles diminishes and the behavior approaches that of a bubbly liquid. We will begin with a

description of the structure of dry foam, which can then be extrapolated towards wet foam under some constraints.

As early as 1873, Joseph Plateau formulated a set of laws for the description of an ideal (dry) foam (Plateau, 1873). These principles have been proved mathematically by Jean Taylor in 1976 (Almgren and Taylor, 1976; Taylor, 1976) and are still valid today. The assumptions for this idealized foam are a very low liquid fraction $10^{-4} < \phi_l < 10^{-2}$, an equilibrium at a local energy minimum, zero thickness films and incompressibility. Plateau's law can then be summarized as (taken from (Cantat, 2013):

- 1) *Equilibrium of faces: the soap films are smooth and have a constant mean curvature which is determined by the Young–Laplace law (Eq. (1)).*
- 2) *Equilibrium of edges: the films always meet in threes along edges, forming angles of $120^\circ = \arccos(-1/2)$.*
- 3) *Equilibrium of vertices: the edges meet four-fold at vertices, forming angles of $\theta_a = \arccos(-1/3) \approx 109.5^\circ \approx 1.91 \text{ rad}$.*

In a monodisperse ordered foam, the individual bubbles then take on the shape of a Kelvin cell, an octahedron with 8 hexagonal and 6 square faces. In real foams, the cells statistically have between 12 and 14 faces, with an average of 5 edges each. The curvature of the faces will depend on the size relations between neighboring cells. According to Eq. (1), smaller cells will have convex walls, larger ones concave walls. The edges of three adjoining faces form the characteristic Plateau borders, the main pathways for liquid transport causing drainage. Four of these channels meet in tetrahedral vertices (at 109.5°) called nodes (see Figure 1). Since the borders have a triangular cross section with concave walls of much smaller curvature than the adjoining films, capillary suction $P_c \approx \gamma/r$ will transport liquid from the films towards the borders. Along with gravity induced drainage, this effect will induce a thinning of the films over time, which eventually leads to the foam aging phenomena of film rupture and cell coalescence.

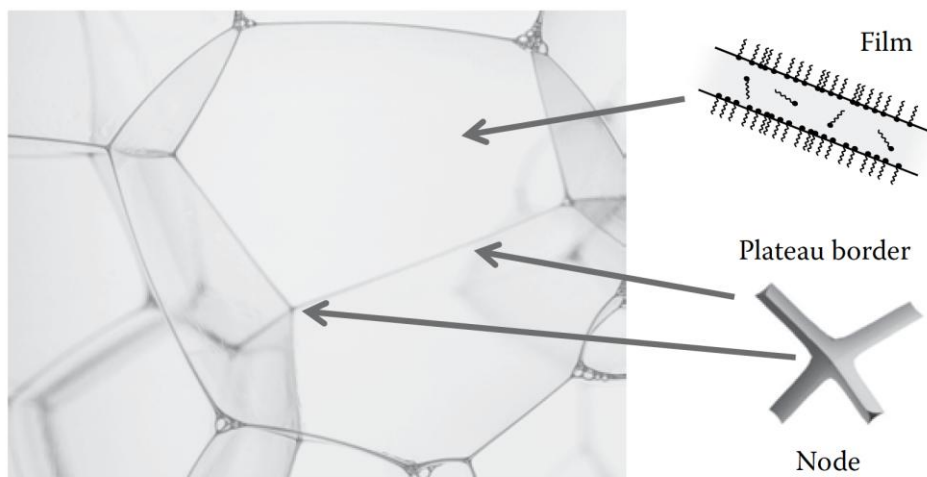


Figure 1: Elements of foam structure, depicted in a polyhedral dry foam (Ekserova et al., 2019)

When the liquid fraction in a foam is increased, the cross-sectional area of the Plateau borders increases at the cost of film area, while the film thickness remains negligibly thin. At a critical liquid fraction ϕ_l^* , the films vanish as opposing borders

$$K_p = \frac{1}{6} \left[\frac{3}{25} + \sqrt{\frac{2}{Bo} \arctan \sqrt{\frac{1}{8Bo}} - \arctan \left(\frac{1}{2\pi Bo} \right)} \right] \quad \text{Eq. (14)}$$

For $Bo \gg 1$, the interface is almost immobile and approaches the behaviour of solid walls (no-slip condition). As shown in Figure 2, it tends towards a value of 0.02, corresponding to pure Poiseuille flow in channels with solid walls.

The validity of such models is very good, as demonstrated in the experiments of (Lorenceau et al., 2009), shown in Figure 3.

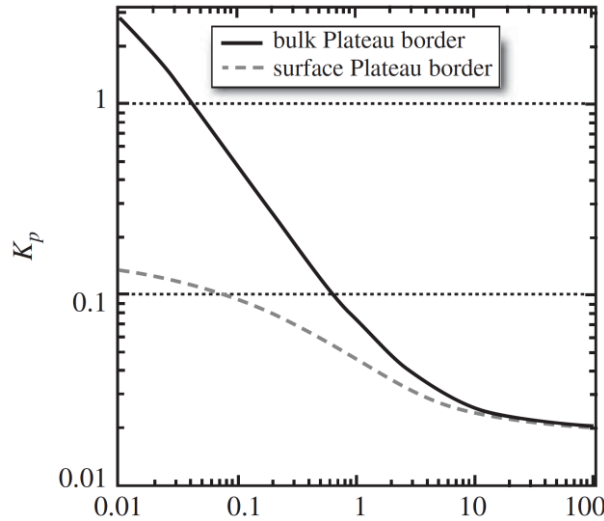


Figure 2: Correlation between Boussinesq-Number and permeability coefficient K_p (Stephan A. Koehler et al., 2004)

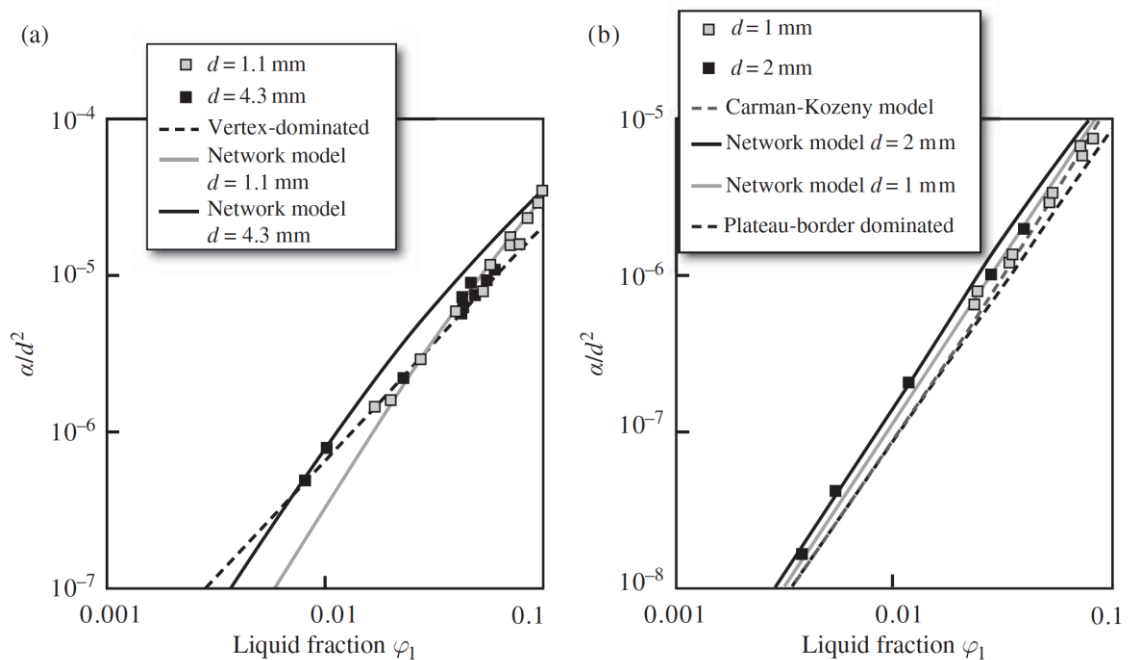


Figure 3: Comparison between models and forced drainage experiments (Lorenceau et al., 2009)

Moving on to the mass transport in the gas phase, foams exhibit an effect similar to Ostwald-ripening found in emulsions or crystal-growth. It is caused by pressure differences across curved cell walls according to the Young-Laplace law. The effect can best be explained in a 2D-case (see Figure 4), where Plateau laws dictate an angle of 120° between contacting faces of a cell. This can only be achieved, if the cell is composed of six faces, which, consequentially, are flat. A number of faces n less than 6 results in a convex deformation and according to Young-Laplace an increase in internal pressure. Thus, gas will diffuse out of the cell through the films, causing the cell to shrink. If, on the contrary, $n > 6$, the faces are concave and the lower internal pressure will provide the driving force for gas from the surrounding bubbles to enter the cell and cause it to grow. In a closed system, the total volume of foam will remain the same, but due to this mechanism, the average bubble size will increase. Additionally, bubbles with $n < 6$ will eventually disappear (described as “T2” event), so the total number of bubbles in the system will decrease.

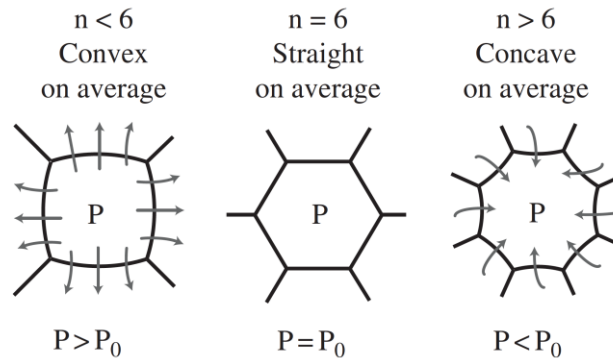


Figure 4: Driving force for coarsening in the 2D case (Cantat, 2013)

The same concept can be transferred to the 3D case, however, in contrast to the 2D case, there is no exact mathematical description available. From experiments and numerical simulations (Thomas et al., 2006), a range of $12 < n < 15$ was found for stable bubbles, $n < 11$ induces shrinkage and $n > 16$ will cause bubbles to grow. A general mathematical description of bubble growth is given in Eq. (15). This can be evaluated by finding a correlation between the number of faces and the geometric charge $q_i(f)$ empirically or from numerical simulations.

$$\frac{dV_i}{dt} = -D_{eff} V_i^{1/3} q_i \quad \text{Eq. (15)}$$

$$\text{with } q_i = \sum \frac{H_{ij} S_{ij}}{V_i^{1/3}} \quad \text{Eq. (16)}$$

V_i = Bubble volume

D_{eff} = Diffusion coefficient

q_i = Geometric charge

H_{ij} = mean curvature of the film

S_{ij} = area of the face separating bubble i and j

A third mechanism changing the foam structure over time is coalescence due to the rupturing of individual foam films. Theoretical knowledge on this phenomenon is far less advanced than for the other two effects described above. What is clear, is that film rupture originates from a disturbance of the equilibrium of van der Waals and repulsive forces. If the disjoining pressure Π_d locally decreases beyond a critical value, it is no longer able to separate the two interfaces and a hole is created. Driven by surface energy minimization, this hole will grow rapidly until the film has completely vanished. If

such a rupture happens within a foam, its shockwaves will usually affect neighbouring films as well and cause an avalanche-like effect, destroying many bubbles in short succession.

There are some theories, aimed at describing the mechanism of individual film rupture. One explanation is the localized depletion of surfactants at the interface caused by drainage or capillary suction in very dry films (Cantat, 2013). Another theory postulates sine-like interface deformations (Vrij, 1966; Vrij and Overbeek, 1968) caused thermal fluctuations that are able to reduce the interface distance below the equilibrium thickness. Another possible cause would be pressure fluctuations, e.g. by acoustic excitation, if the sound pressure exceeds the disjoining pressure. Further research in this area is thus required, in particular considering the importance of this mechanism for applications of forced foam destruction (see chapter 4).

The mechanical behavior of foam under external stresses can be described as viscoelastic with a characteristic yield stress, much like that of individual films. In fact, the processes at the length scale of films are governing the macroscopic behavior. The elastic properties can again best be visualized using a 2D foam model (see Figure 5). At small strains $\epsilon < \epsilon_y$ foam behaves as a soft solid material, according to Hooke's law $\sigma = G\epsilon$ with the shear modulus G . An applied stress will only deform the individual cells, which will return to their original shape once the stress is removed. If the stress increases so that the films parallel to the applied stress align (Figure 5c), the cells can move along these planes and cause plastic deformation (see cell rearrangement in Figure 5d). The deformation of the cells is accompanied by a stretching or compression of the affected films. This induces the need for equilibration of the surfactant concentration at the interface. Mobile interfaces allow that to happen very quickly, resulting in a soft elastic behavior (low shear modulus G), while for rigid interfaces G will increase. A correlation for the elastic shear modulus of polydisperse 3D foams was proposed by Cantat, 2013 as $G \sim \gamma/R_{32} \cdot f(\phi_l)$, showing the dependence on the inverse Sauter mean diameter of bubbles R_{32} and the liquid fraction. An increase of ϕ_l will cause a lower elastic modulus, up until the critical liquid fraction $\phi_l^* \sim 0,36$, where the foam loses inter-bubble contacts and the elastic behavior vanishes. The yield stress of a foam is influenced by the same parameters as the shear modulus and can be modeled according to Eq. (17) (Saint-Jalmes and Durian, 1999).

$$\sigma_y = (0.2 \dots 0.5) \frac{\gamma}{R_{32}} (\phi_l^* - \phi_l)^2 \quad \text{Eq. (17)}$$

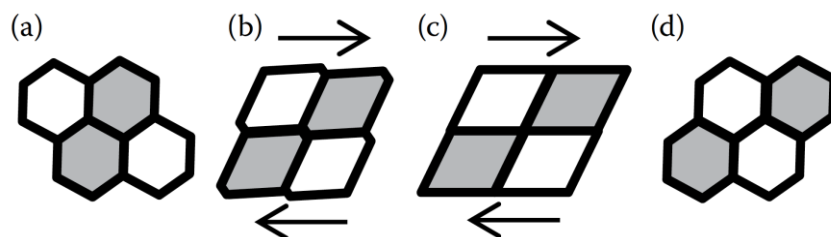


Figure 5: Elastic deformation of a 2D foam (Ekserova et al., 2019)

Above the yield stress, a flowing foam is subject to viscous dissipation due to hydrodynamic effects in the bulk liquid of the films (shear flow) and mass transport of surfactants along the interfaces or from the bulk. Its behaviour can be modelled as a

Maxwell-fluid (spring and slider in parallel with a damper) and the effective viscosity η_{eff} is evaluated according to the Herschel-Bulkley law:

$$\eta_{eff} = \frac{\sigma_y}{\dot{\epsilon}} + \eta_p \dot{\epsilon}^{\beta-1} \quad \text{Eq. (18)}$$

σ_y = Yield stress

$\dot{\epsilon}$ = Strain rate

η_p = Plastic viscosity / consistency

β = Power-law factor (for foams: $\beta < 1 \rightarrow$ shear thinning)

The exponent β again reflects the surface dilatational elasticity of the films. For highly mobile films with low elasticity, $\beta \sim 0.5$, while rigid interfaces decrease the factor to approximately $\beta = 0.2$. The plastic viscosity can be described as a function of surface tension, bubble size, and liquid fraction, but is also directly proportional to interface elasticity.

The frequency response of a foam can also be described by the complex shear modulus $G^*(\omega)$ (see Eq. (8)), a graphical representation is given in Figure 6. At high frequencies, the flow is viscous-dominated, $G'' \gg G'$ and the complex modulus can be derived as $G^*(\omega) = G(1 + \sqrt{i\omega})$. In the elastic regime at intermediate frequencies, G' dominates and the behavior is described by Hooke's law. If the stress is applied even lower, the time-scales of the phenomena of foam ageing (ripening, drainage, coalescence) become dominant and the behavior is characterized by the gradual increase of bubble size (and its influence on mechanical foam properties).

One final particular property of foam flows is the wall interaction. In the case of smooth walls, the films between the outermost cells/bubbles and the walls allow for macroscopic wall-slip to occur. Only if the surface roughness is in the scale of the bubbles, a no-slip condition can be assumed. This has practical implications on flow profiles and has to be accounted for in rheological measurements and apparatus design. The flow within these sheared films can be described by lubrication theory for mobile interfaces (Plateau borders move along the wall-bound films) and by Couette-flow for rigid interfaces. An analogous effect, called shear-banding, can also be observed in foam flow, if the applied stress is in the order of the yield stress. In this case, only a few layers of cells, or planes of aligned films are sufficient to reduce the applied stress to zero. The remainder of the foam will then be transported as a plug flow at constant velocity. At higher stress levels, these different velocity gradients will vanish.

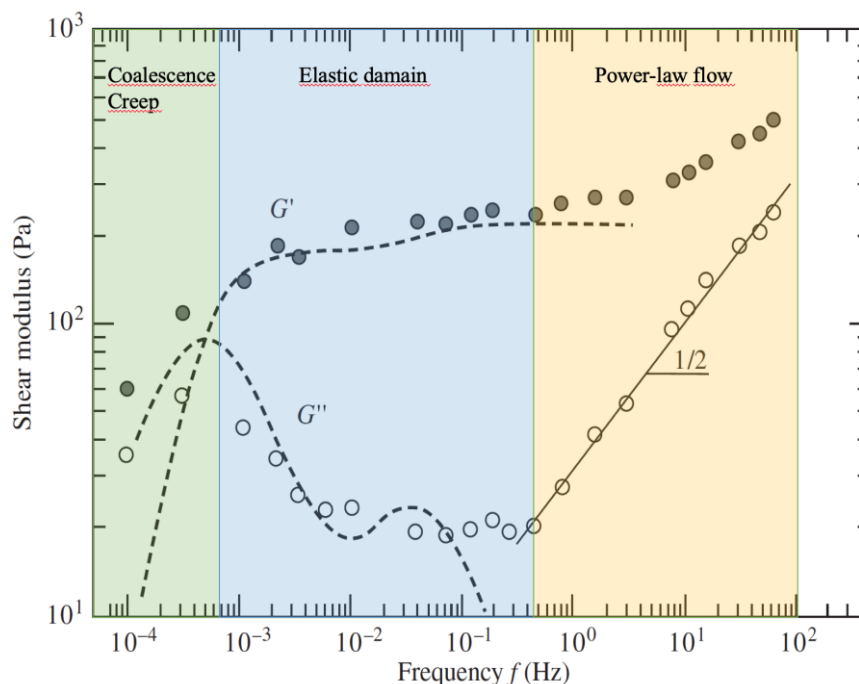


Figure 6: Complex shear modulus of a foam over 7 decades of frequency (Cohen-Addad et al., 2004, 1998; Gopal and Durian, 2003)

3. FOAM MODELLING AND SIMULATION

Previously published predictions for the behavior of flowing foams largely use semi-empirical modelling approaches (Herzhaft et al., 2005; Lauridsen et al., 2004; Yuan and Edwards, 1995). Due to the complexity of the processes, however, these models neglect important effects and mechanisms, for example competing surface processes with surface-active substances (Kotsmar et al., 2009), Ostwald maturation (Drenckhan et al., 2005; Ekblad and Liedberg, 2010), liquid drainage from the plateau channels (S. A. Koehler et al., 2004) or topological changes with sufficiently high deformation energy (Drenckhan and Langevin, 2010; Herzhaft, 2002; Herzhaft et al., 2005). New modelling approaches attempt to take these micromechanical effects into account (Kern et al., 2004; Rouyer et al., 2003; Sun and Hutzler, 2005). Previous works of the authors also encompass modelling of foam growth (Gladbach et al., 2018, 2017) and transport (Zoheidi et al., 2017).

Investigations on the structure of foams and foam cells have been performed using morphological simulations. The most prominent example is Surface Evolver, developed as early as 1992 (Brakke, 1992). It tessellates the films as 2D surfaces and calculated states of minimum energy. The code is able to calculate several thousands of 3D-cells and has provided insights in foam topology, rearrangement details and foam stability. A new approach into the modelling of foam physics at the mesoscale was published by Saye and Sethian (2013). They applied a multiscale approach to model effects of surface tension, gas dynamics, drainage and film rupture based on a Navier-Stokes solver for fluid flow, a finite element approach to simulate film deformation and

Voronoi-tessellation for cell rearrangement. A downside of this approach are very high computational demands, limiting the concept to clusters of only a few cells.

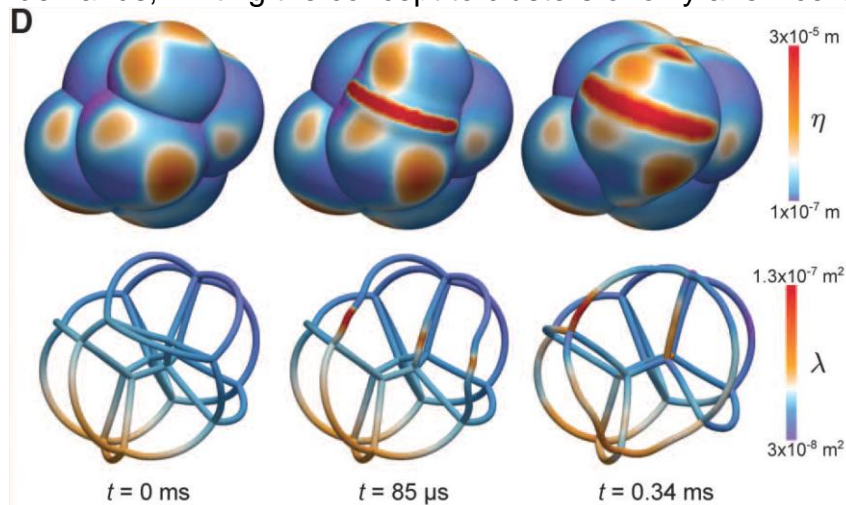


Figure 7: Simulation of film rupture in a small cluster of bubbles (Saye and Sethian, 2013)

Euler-Euler approaches (consideration of foam as a discrete phase) prove to be the first choice for describing foam behavior on a macroscopic level. A consideration of the foam as a homogeneous phase saves computing resources, since there is no resolution of foam topology (lamellae, Plateau borders). This, coupled with a highly parallel code, makes it possible to simulate a foam volume orders of magnitude higher than with conventional (Euler-Lagrange) approaches. In a current project on foam management in industrial plants³, the authors use this approach to simulate the foaming of beverages during bottle filling. It is realized using the „inhomogeneous Multiple Size Group“ (iMUSIG) model implemented by Ansys, which handles dispersed gas in individual classes depending on bubble sizes and allows foam to be introduced as a third component. A first result is shown in Figure 8, demonstrating the simulation of gas entrapment in an impinging jet.

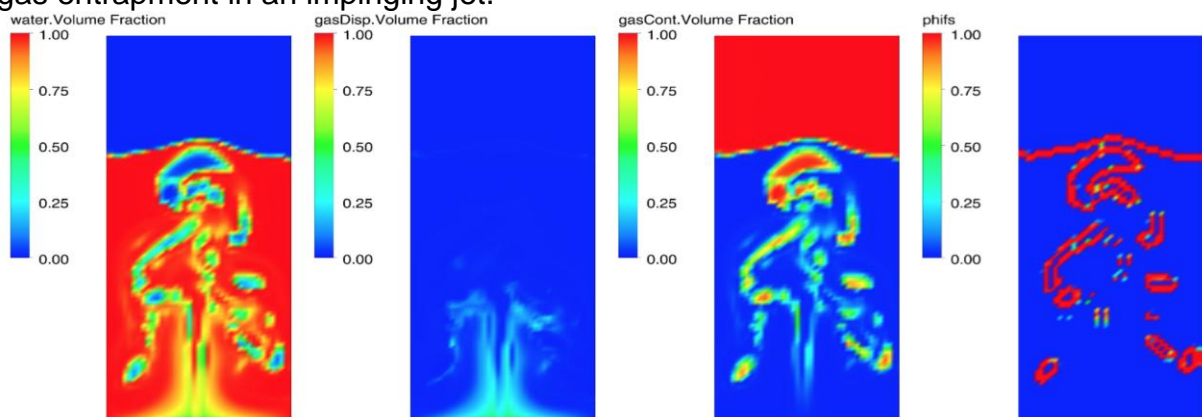


Figure 8: Test geometry for the development and implementation of the foam phase using iMUSIG: volume fraction water, volume fraction of the disperse gas component, volume fraction of the continuous gas component, boundary layer gas-liquid (fltr).

³ <https://www.schaummanagement.de>

The numerical methods employed for these Euler-Euler investigations are typically finite volume (Drew and Passman, 2005; Sattar et al., 2014), finite element (Aloku and Yuan, 2010; Brydon et al., 2005; Rao et al., 2012) or meshless approaches. Of the latter, in particular material point method proved very successful in capturing the mechanics of foam flow (Ram et al., 2015; Yue et al., 2015). Applications of these approaches are typically aimed at the production of foamed materials (polymers, metals, ceramics). Meshless methods can also be employed for simulation of fully resolved foam structures. In particular, the method of smooth particle hydrodynamics (SPH) has been applied to simulate realistic foam behavior (Bender et al., 2018; Busaryev et al., 2012; Cleary et al., 2007; Ihmsen et al., 2012; Thürey et al., 2007). While these examples aim mostly towards 3D-Graphics, the authors of this work aim to implement the concept for engineering tasks in the context of ultrasonic-assisted foam management. A result is shown in Figure 9, which was implemented in GPUSPH (Giuseppe Bilotta, 2014), using a surface tension model by (Grenier et al., 2009).

Finally, the Lattice-Boltzmann method (LBM) offers a very powerful tool for the treatment of foam phenomena, mechanisms and structures over the length scales of proteins up to those of the product (Ge et al., 2007). In a cluster-project coordinated by the authors (Häusser and Kinkel, 2014), this method was applied for mesoscale simulation of flow-induced effects on protein foams by Anderl et al. using an in-house code (waLBerla) (Anderl et al., 2014c, 2014a, 2014b). The massively parallel code was able to simulate effects from the microscale (protein adsorption at the interface) through the mesoscale (bubble formation and interaction) to macroscopic foam transport in channel flows.

The amount of data resulting from such numerical simulations can be extensive and the necessary computer equipment are usually not available in industrial practice. Thus, the application of these results can be greatly facilitated by the use of knowledge-based models and data reduction. Literature suggests various methods for this purpose attributing a relevant potential to artificial neuronal networks (ANN), see also (Arnold et al., 2002; Kurz et al., 1953; Rauh et al., 2012).

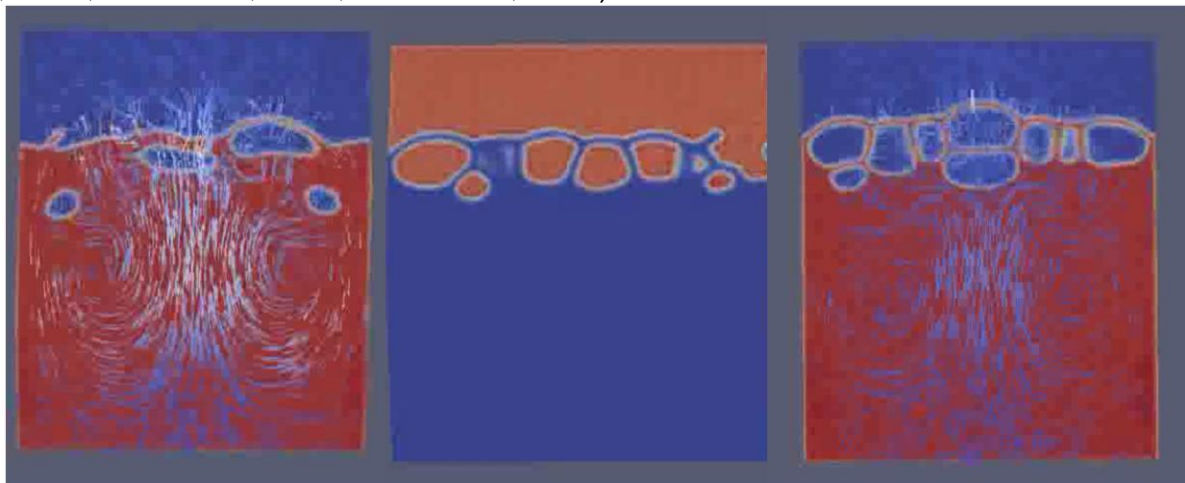


Figure 9: SPH simulation of bubble rising, foam formation and coalescence performed in GPUSPH. The images from left to right show the effect of reduced surface tension (rapid coalescence left, stable foam right).

ANNs are adaptive, nonlinear universal approximators that can predict outputs by combining input parameters through hidden layers (sigmoid functions) weighted functions. The concept of ANNs originate in the human nervous system and they are able to predict the behavior of a system, recognize patterns, and perform optimization and control functions. In a project on the stabilization of protein foams in food technology (Häusser and Kinkel, 2014), they were used as functional units to approximate data sets from experimental or numerical calculations. ANN are first trained in a phase in which the system learns, i.e. deviations in their output compared to the original data are minimized. The ANN are then validated with another set of data to ensure that the accuracy of the prediction is the same. Finally, they are tested by evaluating unknown data for the quality of the statements.

In this project the ANN were first trained to approximate the relationship between a protein concentration and pH value with surface tension. It could be shown that the ANN predicted the desired correlation with a maximum mean square error of between 0.006 and 0.034. Furthermore, specific ANNs were used to predict experimental data of foamability, foam stability, foam capacity and drainage for solutions with sodium caseinate, β -lactoglobulin and micellar casein, again with mean square errors of 0.0025 to 0.048.

The ANNs also made it possible to predict the processes involved in the transport of foam through internal geometries such as pipes or ducts. Here, the strategy of data and model reduction was to generate a fingerprint of the convective transport processes. For this purpose, the pipe was divided into input, middle and output areas. Each area was divided into an inner, upper, lower and lateral area, resulting in 12 areas for prediction. The behavior of the transport in each area was described by the three components of velocity, gas volume fraction and shear stress. These three physical properties were obtained for different viscosities and surface tensions of the liquid phase of the foam. The basis of the data set for ANN training were simulations of foam transport in a channel section using the Lattice-Boltzmann method. Finally, the velocity component in the transport direction could be predicted by ANNs with a maximum mean square error of 0.2 and a minimum correlation of 82%, while the velocity components normal to the flow direction could be defined with a maximum mean square error of 0.028 or 0.07 and a minimum correlation of 95 % or 75 %, respectively. Consequently, the physical properties of a foam could be predicted satisfactorily by ANNs trained with experimental data. In the same way, the results of numerical simulations allowed for predictive mapping of foam transport in a square section. After teaching and validation, the code for the ANNs can be executed on any workstation or even higher-end microcontrollers, thus allowing an easy transfer of knowledge gained through scientific investigations (experimental and numerical) to practical operation of reactors and plants.

4. ACTIVE FOAM DESTRUCTION TECHNIQUES

The technical production of fine chemicals as well as food and beverages often leads to undesired foam formation. This often causes substantial changes in mass, impulse and energy transport as well as (bio-) chemical conversions up to a complete

obstruction of processing. The effects range from increased pressure losses and energy requirements to reduced throughput and separation performance. Among the most affected reactors are columns, scrubbers, mash vessels, fermentation tanks, stirrers, evaporators and combustion bubbles. However, foam management is usually not a large focus of process and equipment design. The very high time and cost pressure on the one hand, coupled with the lack of predictive and diagnostic tools, makes it difficult to detect foam during operation and to implement solutions. Due to the formation of stable secondary foams, frequently used mechanical foam destroyers do not solve the problem. The use of defoaming agents as additives is also subject to severe restrictions with regard to product purity and safety, costs and complex separation operations.

For any form of physical foam management, the dynamic net foam balance plays an important role.

$$\text{DNFB} = \sum \text{Foam generating effects} - \sum |\text{Foam removing effects}| \quad \text{Eq. (19)}$$

Only negative values of this balance within an apparatus prevent the formation of disturbing foam covers. Furthermore, for an efficient foam management, the ratio of the characteristic process time and the foam existence time need to be considered. This can be achieved by observing the generalized Deborah number:

$$\text{De} = \frac{\text{Characteristic processing time}}{\text{Characteristic time of foam decay}} \quad \text{Eq. (20)}$$

An ideal destruction method reduces the characteristic time of existence to such an extent that no foam occurs within the process time.

Foam destruction. Published literature proposes acoustic, thermal and mechanical methods for forced physical foam destruction (Miller, 2008; Pahl and Franke, 1995; Vardar-Sukan, 1998; Zlokarnik, 1999). Mechanical approaches such as rotating and spin-inducing elements entail high investment and operating costs. They increase the drainage by applying additional mass forces, but lead to a very stable secondary foam, which cannot further be destroyed mechanically. Irrigation of foam layers with liquid droplets shows clear advantages in these aspects, but also leads to secondary foaming under certain operating conditions (Pahl and Franke, 1995; Pahl and Meinecke, 1989; Zlokarnik, 1999).

For the acoustic foam destruction of particular interest in this paper, the literature discusses various alternatives based on different mechanisms of action. (Awad et al., 2012) suggest bubble destruction by means of induced cavitation (Da-Wen, 2005; Gallego-Juárez et al., 2010; Rodríguez et al., 2010), which is already used in practice (e.g. Cavitus⁴). The decisive disadvantages of cavitation-related foam control are the potential physical-chemical product degradations and aerosol formation, which are hardly controllable due to the high energies released by imploding cavitation bubbles (pressures in the MPa range and temperatures of thousands of Kelvin!). The second alternative is based on a theory of the formation of surface waves that accelerate drainage through local fluctuations in lamella thickness (Barigou, 2001; Dedhia et al., 2004; Morey et al., 1999; Sandor and Stein, 1993; Winterburn and Martin, 2009). The third alternative, used in a current project by the authors, uses ultrasonic waves to excite the foam lamellae in their eigenmode, causing them to fail mechanically. For a

⁴ www.cavitus.com

sensible choice of the frequency bandwidth of such an actuator, the resonance frequencies f_R of the bubbles with radius R_0 can be calculated from the surface tension σ , viscosity η and density ρ through the Rayleigh-Plesset equation.

$$f_{R,RP} = \frac{1}{2\pi r_R} \sqrt{\frac{3\gamma \left(p_0 + \frac{2\sigma}{r_R}\right) - \frac{2\sigma}{r_R}}{\rho_{Fluid}}} \quad \text{Eq. (21)}$$

The resonance behavior of the bubbles for different juices was thus evaluated within the project (Figure 10). The lowest ultrasonic frequency of 20 kHz and the natural frequency of the smallest realistic foam bubble were used as the limits of the initially assumed frequency range. It was shown that a frequency between 20 and 100 kHz seems to be suited well for the bubble sizes usually found in detrimental foams. Studies by (Medwin, 1977) and (Sarkar and Prosperetti, 1994, 1993) postulate a similar frequency range for water in which bubbles absorb ultrasound particularly strongly. In addition, the publications predict relatively narrow bubble size ranges that can be brought into resonance with a given frequency.

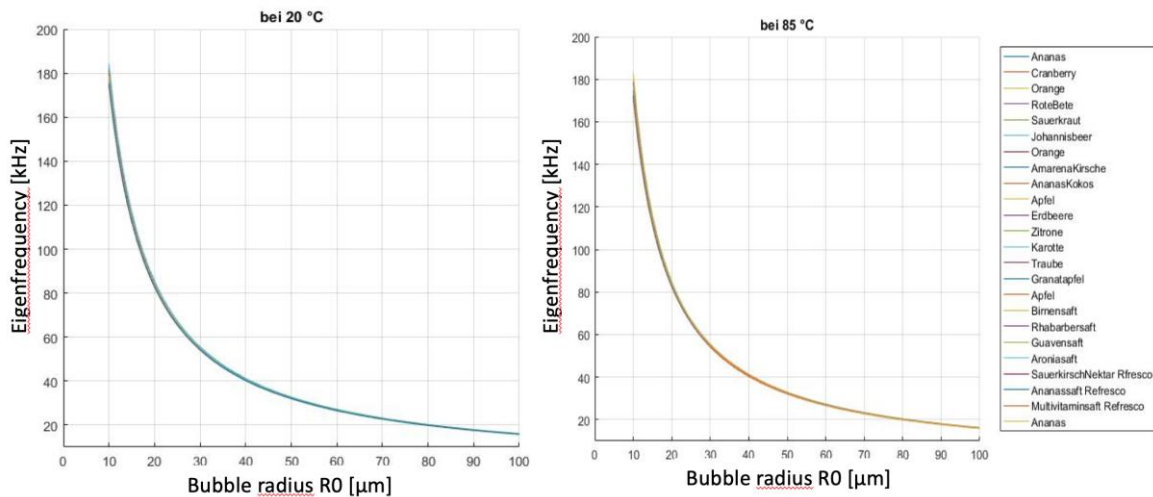


Figure 10: Calculated Eigenfrequencies of bubbles in fruit juices according to the Rayleigh-Plesset equation Eq. (21)

For an experimental validation of the concept, a 400 mm wide plexiglass column was used, to which plate transducers (80, 120 and 250 kHz) were attached at the level of the liquid level. For foaming, air was pumped into the liquid (blackcurrant juice) via a perforated ring at the bottom of the column. The foaming phase was completed after a foam height of 20 cm had been reached, this took 12 +/- 3 s in all tests. Experiments were carried out using all three transducers, with only two frequencies (80 and 120 kHz), as well as without ultrasound. The frequencies were activated in chronological order, starting with the highest frequency and changed to the next lower frequency after 30 seconds.

In all experiments a continuous foam decay could be observed (see Figure 11 and Figure 12). In the experiments without ultrasound, foam stability was very high, resulting in a decay time of 27 minutes and residual foam covering 48 % of the liquid surface. When only two transducers were used, a much faster foam decay was found. The series of tests could be completed after 1200 s, when no further decay could be detected and the foam residue was 20 %. With the activation of all three transducers,

the foam was initially decomposed as quickly as with only two frequencies. However, after about half of the foam had decayed, the foam decayed steadily at a lower rate down to about 5% residual surface coverage.

The foam destruction by long-wave thermal radiation proposed here as a further alternative is dealt with in the literature in the context of fire fighting, e.g. (Chhabra and De Kee, 1993). Mechanistically, this type of foam destruction is based on (i) the evaporation of the lamella liquid, (ii) the reduction of its viscosity and the resulting accelerated drainage and (iii) an increase in pressure inside the gas bubbles (Pahl and Franke, 1995). Other defoaming methods with severely limited applicability use laser radiation and microwaves.

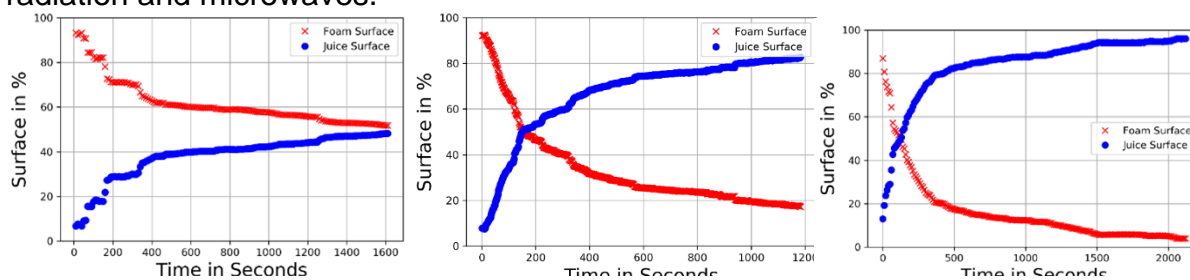


Figure 11: Time series of the surface fraction of foam residue and exposed currant juice: reference measurement without ultrasound (left), ultrasound test with 80 & 120 kHz (middle) and ultrasound test with 80, 120 & 250 kHz.



Figure 12: Visual evaluation of the foam decay with frequencies 80, 120 & 250 kHz from test start in 5 second steps (from left to right).

5. CONCLUSIONS

Foams are inherently metastable systems in which gas is dispersed in a liquid or solid phase. Their behavior is dominated by surface effects at the microscale, dictating their spatio-temporal properties all the way to the macroscale. The metastability of foam is characterized by a temporal evolution of its structure caused by the phenomena of coarsening, drainage and coalescence. This means that foam will increase its average bubble size over time, it will reduce its liquid content and the total number of bubbles contained in a foam will gradually decrease, and reach zero at infinity. The mechanical properties of foam can be described as viscoelastic, indicating that foam will act as a very soft solid material under low stress and flow under the constraints of viscous dissipation above a characteristic yield stress. The elastic behavior results from geometric constraints between the foam cells, causing their (reversible) deformation up

until the fluid films align to form shear layers. The rheology can be modelled with good accuracy using the Herschel-Bulkley law.

For the modelling of the non-equilibrium behavior of foam, empirical / phenomenological models show limited success due to the complexity of the effects involved. For engineering approaches, Euler-Euler simulations have been employed to some success, reducing foam to a distinct phase with modelled properties. A resolution of the complex foam structure on a practical level has so far only been achieved using meshless methods, such as Lattice Boltzmann Simulations. In order to transfer the insights of such scientific investigations to industrial end-users, the application of a hybrid knowledge-based approach based on artificial neural networks (ANN) was successfully demonstrated by the authors for the stabilization of protein foams in food technology. Using this concept of in-depth experimental and numerical investigations, combined with a transfer using ANNs, the authors currently develop foam management strategies for industrial processes where foam is unwanted or harmful. First exemplary results show the good performance of ultrasound induced foam reduction, as one of the investigated methods.

REFERENCES

- de Almeida, R.M.C., Mombach, JoséC.M., 1997. *Phys. Stat. Mech. Its Appl.* 236, 268–278.
- Almgren, F.J., Taylor, J.E., 1976. *Sci. Am.* 235, 82–93.
- Aloku, G.O., Yuan, X.-F., 2010. *Chem. Eng. Sci.* 65, 3749–3761.
- Anderl, D., Bauer, M., Rauh, C., Råde, U., Delgado, A., 2014a. *Food Funct.* 5, 755–763.
- Anderl, D., Bauer, M., Rauh, C., Råde, U., Delgado, A., 2014b. *PAMM* 14, 667–668.
- Anderl, D., Bogner, S., Rauh, C., Råde, U., Delgado, A., 2014c. *Comput. Math. Appl.* 67, 331–339.
- Arnold, S., Becker, T., Delgado, A., Emde, F., Enenkel, A., 2002. *J. Biotechnol.* 97, 133–145.
- Awad, T.S., Moharram, H.A., Shaltout, O.E., Asker, D., Youssef, M.M., 2012. *Food Res. Int.* 48, 410–427.
- Barigou, M., 2001. *Chem. Eng. Technol. Ind. Chem.-Plant Equip.-Process Eng.-Biotechnol.* 24, 659–663.
- Bender, J., Koschier, D., Kugelstadt, T., Weiler, M., 2018. *IEEE Trans. Vis. Comput. Graph.* 1–1.
- Brakke, K.A., 1992. *Exp. Math.* 1, 141–165.
- Brydon, A.D., Bardenhagen, S.G., Miller, E.A., Seidler, G.T., 2005. *J. Mech. Phys. Solids* 53, 2638–2660.
- Busaryev, O., Dey, T.K., Wang, H., Ren, Z., 2012. *ACM Trans. Graph.* 31, 1–8.
- Cantat, I., 2013. *Foams: structure and dynamics*, First English edition. ed. Oxford University Press, Oxford ; New York, NY, United States of America.
- Chhabra, R.P., De Kee, D., 1993. *Dry. Technol.* 11, 263–264.
- Cleary, P.W., Pyo, S.H., Prakash, M., Koo, B.K., 2007. *ACM Trans. Graph.* 26, 97.
- Cohen-Addad, S., Hoballah, H., Höhler, R., 1998. *Phys. Rev. E* 57, 6897.
- Cohen-Addad, S., Höhler, R., Khidas, Y., 2004. *Phys. Rev. Lett.* 93, 028302.

- Dan, A., Kotsmar, C., Ferri, J.K., Javadi, A., Karbaschi, M., Krägel, J., Wüstneck, R., Miller, R., 2012. *Soft Matter* 8, 6057–6065.
- Da-Wen, S., 2005. *Emerging technologies for food processing*. Academic Press, S.L.
- De Gennes, P.-G., Brochard-Wyart, F., Quéré, D., 2013. *Capillarity and wetting phenomena: drops, bubbles, pearls, waves*. Springer Science & Business Media.
- Dedhia, A.C., Ambulgekar, P.V., Pandit, A.B., 2004. *Ultrason. Sonochem.* 11, 67–75.
- Derjaguin, B.V., Churaev, N.V., Muller, V.M., 1987a. The Derjaguin—Landau—Verwey—Overbeek (DLVO) theory of stability of lyophobic colloids, in: *Surface Forces*. Springer, pp. 293–310.
- Derjaguin, B.V., Churaev, N.V., Muller, V.M., 1987b. *Surface forces*. Consult. Bureau. Plenum Pub. Co., New York.
- Drenckhan, W., Cox, S.J., Delaney, G., Holste, H., Weaire, D., Kern, N., 2005. *Colloids Surf. Physicochem. Eng. Asp.* 263, 52–64.
- Drenckhan, W., Langevin, D., 2010. *Curr. Opin. Colloid Interface Sci.* 15, 341–358.
- Drew, D.A., Passman, S.L., 2005. *Theory of multicomponent fluids*. Springer, New York.
- Ekblad, T., Liedberg, B., 2010. *Curr. Opin. Colloid Interface Sci.* 15, 499–509.
- Ekserova, D.R., Gochev, G., Platikanov, D., Liggieri, L., Miller, R., 2019. *Foam films and foams: fundamentals and applications*.
- Engelhardt, K., Lexis, M., Gochev, G., Konnerth, C., Miller, R., Willenbacher, N., Peukert, W., Braunschweig, B., 2013. *Langmuir* 29, 11646–11655.
- Engelhardt, K., Rumpel, A., Walter, J., Dombrowski, J., Kulozik, U., Braunschweig, B., Peukert, W., 2012. *Langmuir* 28, 7780–7787.
- Fainerman, V.B., Lucassen-Reynders, E.H., Miller, R., 2003. *Adv. Colloid Interface Sci.* 106, 237–259.
- Fainerman, V.B., Miller, R., 1996. *Langmuir* 12, 6011–6014.
- Fainerman, V.B., Miller, R., 2009. Adsorption isotherms at liquid interfaces, in: *Encyclopedia of Surface and Colloid Science*. Taylor & Francis.
- Fainerman, V.B., Miller, R., Wüstneck, R., Makievski, A.V., 1996. *J. Phys. Chem.* 100, 7669–7675.
- Fainerman, V.B., Wüstneck, R., Miller, R., 2001. *Tenside Surfactants Deterg.* 38, 224–229.
- Frumkin, A., 1925. *Z. Für Phys. Chem.* 116, 466–484.
- Gallego-Juárez, J.A., Rodriguez, G., Acosta, V., Riera, E., 2010. *Ultrason. Sonochem.* 17, 953–964.
- Ge, W., Chen, F., Gao, J., Gao, S., Huang, J., Liu, X., Ren, Y., Sun, Q., Wang, L., Wang, W., 2007. *Chem. Eng. Sci.* 62, 3346–3377.
- Gibbs, J.W., 1928. *The collected works of JW Gibbs*. Longmans, Green.
- Giuseppe Bilotta, 2014. GPU implementation and validation of fully three-dimensional multi-fluid SPH models (No. Rapporto Tecnico 292), INGV.
- Gladbach, K., Delgado, A., Rauh, C., 2017. *World J. Mech.* 7, 297–322.
- Gladbach, K., Delgado, A., Rauh, C., 2018. *World J. Mech.* 8, 417.
- Gopal, A.D., Durian, D.J., 2003. *Phys. Rev. Lett.* 91, 188303.
- Grenier, N., Antuono, M., Colagrossi, A., Le Touzé, D., Alessandrini, B., 2009. *J. Comput. Phys.* 228, 8380–8393.

- Häusser, V., Kinkel, D. (Eds.), 2014. Proteinschäume in der Lebensmittelproduktion: Mechanismenaufklärung, Modellierung und Simulation: 2011-2014. Forschungskreis der Ernährungsindustrie, Bonn.
- Henry, W., 1803. Philos. Trans. R. Soc. Lond. 29–274.
- Herzhaft, B., 2002. J. Colloid Interface Sci. 247, 412–423.
- Herzhaft, B., Kakadjian, S., Moan, M., 2005. Colloids Surf. Physicochem. Eng. Asp. 263, 153–164.
- Ihmsen, M., Akinci, N., Akinci, G., Teschner, M., 2012. Vis. Comput. 28, 669–677.
- Israelachvili, J.N., 2015. Intermolecular and surface forces. Academic press.
- Kern, N., Weaire, D., Martin, A., Hutzler, S., Cox, S.J., 2004. Phys. Rev. E 70, 041411.
- Koehler, Stephan A., Hilgenfeldt, S., Stone, H.A., 2004. J. Colloid Interface Sci. 276, 420–438.
- Koehler, S. A., Hilgenfeldt, S., Weeks, E.R., Stone, H.A., 2004. J. Colloid Interface Sci. 276, 439–449.
- Kotsmar, C., Pradines, V., Alahverdijeva, V.S., Aksenenko, E.V., Fainerman, V.B., Kovalchuk, V.I., Krägel, J., Leser, M.E., Noskov, B.A., Miller, R., 2009. Adv. Colloid Interface Sci. 150, 41–54.
- Kurz, T., Fellner, M., Becker, T., Delgado, A., 1953. J. Inst. Brew. 59, 241–252.
- Langmuir, I., 1917. J. Frankl. Inst. 184, 721.
- Lauridsen, J., Chanan, G., Dennin, M., 2004. Phys. Rev. Lett. 93, 018303.
- Leonard, R.A., Lemlich, R., 1965. AIChE J. 11, 18–25.
- Lorceau, E., Louvet, N., Rouyer, F., Pitois, O., 2009. Eur. Phys. J. E 28, 293–304.
- Medwin, H., 1977. Ultrasonics 15, 7–13.
- Miller, C.A., 2008. Curr. Opin. Colloid Interface Sci. 13, 177–182.
- Morey, M.D., Deshpande, N.S., Barigou, M., 1999. J. Colloid Interface Sci. 219, 90–98.
- Pahl, M.H., Franke, D., 1995. Chem. Ing. Tech. 67, 300–312.
- Pahl, M.H., Meinecke, H., 1989. Dechema-Monogr. 114, 433.
- Plateau, J., 1873. Statique expérimentale et théorique des liquides soumis aux seules forces moléculaires, par J. Plateau, ... Gauthier-Villars, Paris.
- Ram, D., Gast, T., Jiang, C., Schroeder, C., Stomakhin, A., Teran, J., Kavehpour, P., 2015. Proceedings of the 14th ACM SIGGRAPH / Eurographics Symposium on Computer Animation - SCA '15, pp. 157–163.
- Rao, R.R., Mondy, L.A., Noble, D.R., Moffat, H.K., Adolf, D.B., Notz, P.K., 2012. Int. J. Numer. Methods Fluids 68, 1362–1392.
- Rauh, C., Singh, J., Nagel, M., Delgado, A., 2012. Int. Dairy J. 26, 2–14.
- Rodríguez, G., Riera, E., Gallego-Juárez, J.A., Acosta, V.M., Pinto, A., Martínez, I., Blanco, A., 2010. Phys. Procedia 3, 135–139.
- Rouyer, F., Cohen-Addad, S., Vignes-Adler, M., Höhler, R., 2003. Phys. Rev. E 67, 021405.
- Saint-Jalmes, A., Durian, D.J., 1999. J. Rheol. 43, 1411–1422.
- Sandor, N., Stein, H.N., 1993. J. Colloid Interface Sci. 161, 265–267.
- Sarkar, K., Prosperetti, A., 1993. J. Acoust. Soc. Am. 93, 3128–3138.
- Sarkar, K., Prosperetti, A., 1994. J. Acoust. Soc. Am. 96, 332–341.
- Sattar, M.A., Naser, J., Brooks, G., 2014. Chem. Eng. Sci. 107, 165–180.
- Saye, R.I., Sethian, J.A., 2013. Science 340, 720–724.

- Stevenson, P., 2012. Foam engineering: fundamentals and applications. Wiley-Blackwell, Chichester.
- Sun, Q., Hutzler, S., 2005. Colloids Surf. Physicochem. Eng. Asp. 263, 27–32.
- Taylor, J.E., 1976. Ann. Math. 489–539.
- Thomas, G.L., De Almeida, R.M.C., Graner, F., 2006. Phys. Rev. E 74, 021407.
- Thürey, N., Sadlo, F., Schirm, S., Müller-Fischer, M., Gross, M., 2007. Proceedings of the 2007 ACM SIGGRAPH/Eurographics Symposium on Computer Animation, SCA '07. Eurographics Association, Aire-la-Ville, Switzerland, Switzerland, pp. 191–198.
- Vardar-Sukan, F., 1998. Biotechnol. Adv. 16, 913–948.
- Verwey, E.J.W., Overbeek, J.T.G., Van Nes, K., 1948. Theory of the stability of lyophobic colloids: the interaction of sol particles having an electric double layer. Elsevier Publishing Company.
- Vrij, A., 1966. Discuss. Faraday Soc. 42, 23–33.
- Vrij, A., Overbeek, J.T.G., 1968. J. Am. Chem. Soc. 90, 3074–3078.
- Winterburn, J.B., Martin, P.J., 2009. Asia-Pac. J. Chem. Eng. 4, 184–190.
- Wolf, A., Rauh, C., Delgado, A., 2016. Arch. Appl. Mech. 86, 979–1002.
- Wüstneck, R., Fainerman, V.B., Aksenenko, E.V., Kotsmar, Cs., Pradines, V., Krägel, J., Miller, R., 2012. Colloids Surf. Physicochem. Eng. Asp. 404, 17–24.
- Yuan, X.F., Edwards, S.F., 1995. J. Non-Newton. Fluid Mech. 60, 335–348.
- Yue, Y., Smith, B., Batty, C., Zheng, C., Grinspun, E., 2015. ACM Trans. Graph. 34, 1–20.
- Zlokarnik, M., 1999. Rührtechnik. Springer Berlin Heidelberg, Berlin, Heidelberg.
- Zoheidi, L., Panradl, C., Rauh, C., Delgado, A., 2017. J. Food Process Eng.